Surface & Coatings Technology 422 (2021) 127570

Contents lists available at ScienceDirect

Surface & Coatings Technology

journal homepage: www.elsevier.com/locate/surfcoat

Influence of Fe-rich intermetallics and their segregation on anodising properties of Al-Si-Mg rheocast alloys

Baiwei Zhu [a,b], Caterina Zanella [a,c,*]

[a] Department of Materials and Manufacturing, School of Engineering, Jönköping University, P. O. Box 1026, Gjuterigatan 5, SE-551 11 Jönköping, Sweden
[b] School of Mechanical Engineering and Rail Transit, Changzhou University, Changzhou 213164, PR China
[c] Department of Industrial Engineering, Trento University, via Sommarive 9, 38123 Trento, Italy

ARTICLE INFO

Keywords:
Fe-rich intermetallics
Rheocasting
Anodising
Corrosion protection

ABSTRACT

During rheocasting of Al alloys, the component's surface can be enriched in Fe-rich intermetallics due to the surface liquid segregation or the interaction with the die material. Although this precipitates enrichment affects only the surface, it can have a big impact on the quality of the surface treatments or durability. In this paper, the effect of Fe-rich intermetallics on the hardness and corrosion resistance of the anodized layer of AlSiMg alloys was examined by using nanoindentation and electrochemical impedance spectroscopy (EIS) techniques. A sulfuric acid anodising process was performed on unground and mechanical ground surfaces of TX630 substrates produced by the rheocasting process. During anodising, Fe-rich intermetallics can be dissolved, leaving voids in the oxide during its growth. The anodised samples with two different oxide layer thickness (4 and 7 μm) were tested by EIS in 3 wt-% NaCl solution for 12 h. A comparison of the EIS results of unground and mechanically ground surfaces demonstrated that the mechanical grinding successfully removed the Fe enriched layer, improving corrosion protection of the anodised oxide. Moreover, the hardness measurements indicate that the oxide layer on the mechanically ground surface with low Fe content shows higher hardness than on the unground surface with high Fe content.

1. Introduction

Al-Si-Mg alloys are extensively used to manufacture structural components in automotive industries, as they provide good mechanical properties with reduced weight. Such components very often need also to meet the requirements of good corrosion and wear resistance. To meet such requirements, surface treatments such as anodising is commonly performed on the components. Previous studies have revealed that the oxide layer and its performance are strongly depending on the chemical composition [1–4], microstructure [2,5–8], pre-treatments [4,9], the anodising process [8,10–14] and post-treatment [7,15–17].

Fe is commonly found in Al—Si alloys because of the recycling process and casting process, and the presence of Fe helps to prevent die soldering in high pressure die casting (HPDC) process. However, Fe can be considered an undesired alloying element, as it forms Fe-rich intermetallics such as plate-like β-Al_5FeSi particles resulting in a degradation of ductility and corrosion resistance [18–20]. In terms of anodising, Fe is also believed to diminish the specular brightness of the anodised surface, even when present in small amounts [21]. Recent researches have demonstrated the correlation between Fe-rich intermetallics and anodising behaviour, as well as anodising properties. Researchers found that Fe-rich intermetallics can be partly dissolved during anodising, leaving voids and surface defects resulting in a degradation of corrosion resistance of the oxide layer [5,6]. Jariyaboon et al. [16] indicated that the partial dissolution of Fe-rich intermetallics depends on their chemical composition. However, most of these studies concern wrought Al alloys. During semi-solid metal (SSM) processing, such as rheocasting of Al—Si alloys, the surface of the component can be further enriched in Fe-rich intermetallics due to the surface liquid segregation (SLS) or interaction with die material. Previous work by Zhu et al. [8] studied the influence of macrosegregation on surface properties of anodised rheocastings. Results shows that no Fe-rich intermetallics was observed in the cross-section of the oxide layer, and it was believed that the Fe-rich intermetallics on the surface could partly dissolve during anodising. However, detailed studies regarding the mechanism of Fe-rich intermetallics during anodising and the influence of Fe-rich

* Corresponding author at: Department of Materials and Manufacturing, School of Engineering, Jönköping University, P. O. Box 1026, Gjuterigatan 5, SE-551 11 Jönköping, Sweden.
E-mail address: Caterina.Zanella@ju.se (C. Zanella).

https://doi.org/10.1016/j.surfcoat.2021.127570
Received 12 October 2020; Received in revised form 27 July 2021; Accepted 28 July 2021
Available online 31 July 2021

Table I
Chemical composition of Al—7Si.0.4 Mg measured by an optical emission spectroscopy.

Alloy	Si	Mg	Cu	Fe	Mn	Sr
Average [wt-%]	7.200	0.410	0.048	0.120	0.020	0.029
SD	0.035	0.017	0.002	0.006	0.001	0.001

Table II
The oxide layer with the anodising parameters.

Surface preparation	20 V	25 V
Unground	30 min: 3.4 ± 0.8 μm	25 min: 3.5 ± 0.9 μm
	60 min: 7.1 ± 1.5 μm	50 min: 7.4 ± 1.7 μm
Mechanical ground	25 min: 3.9 ± 0.9 μm	20 min: 4.3 ± 0.8 μm
	50 min: 6.9 ± 0.9 μm	30 min: 6.9 ± 0.9 μm

intermetallics on hardness and corrosion resistance need to be conducted.

This paper aims to give a clear demonstration of the mechanism of Fe-rich intermetallics during anodising, and to identify the influence of Fe content and Fe-rich intermetallics on hardness and corrosion resistance of the oxide layer.

2. Experimental

2.1. Materials and casting

Al-7Si-0.4 Mg alloy with an addition of 250 ppm Sr was used (Table I). The addition of Sr aims to modify the Si particles morphology from interconnected plates to disconnected fibres and improve the oxide layer's quality [2,3]. An SSM processing, the RheoMetal™ process [22], was used to produce the samples for investigation. A detailed description of the casting process is given in [8,22]. In the current study, T5 heat treatment was performed within 24 h after casting and quenching in water at room temperature. The artificial ageing process was carried out using an air circulation furnace at the temperature of 175 °C with 4.5 h as holding time, based on a previous study where the optimisation of the heat treatment process was made [23].

2.2. Anodising

Prior to anodising, to remove the Fe-rich IM rich skin, samples were mechanically ground using 1000-grade SiC paper to remove a maximum of 20 μm from the surface. Before anodising, all samples were ultrasonically cleaned in ethanol for 5 min. The anodising process was performed in 1.0 M H_2SO_4 at two constant controlled voltage values of 20 and 25 V at room temperature. The duration of anodising varied from 15 to 50 min in order to obtain two different oxide layer thicknesses (shown in Table II). After anodising, the samples were ultrasonically rinsed in distilled water and dried at 50 °C. The previous study by Zhu et al. [7] showed that, for cast Al—Si alloys, the hydrothermal sealing step reduces the protection capability of the oxide layer. Thus, in the current study, no sealing step was performed after anodising.

2.3. Microstructural characterisation

Microstructural characterisation of the Al-Si-Mg substrates and the oxide layer was examined by optical microscopy (OM, Olympus GX71F) and scanning electron microscopy (FIB-SEM, Tescan LYRA3) equipped with energy dispersive X-ray spectroscopy (EDXS). Before microstructural characterisation, the samples were cut by a diamond saw with low speed and low load to avoid damaging the oxide layer. To characterise the oxide layer's microstructural features and corrosion pits in the cross-section view, a Gatan Ion Polishing system was applied to cross-section and polish the oxide layer before SEM investigation.

2.4. Hardness

Hardness measurements of the oxide layer were carried out using Micro Materials NanoTest Vantage machine equipped with Berkovich hardness indentor. The hardness measurement was performed in the

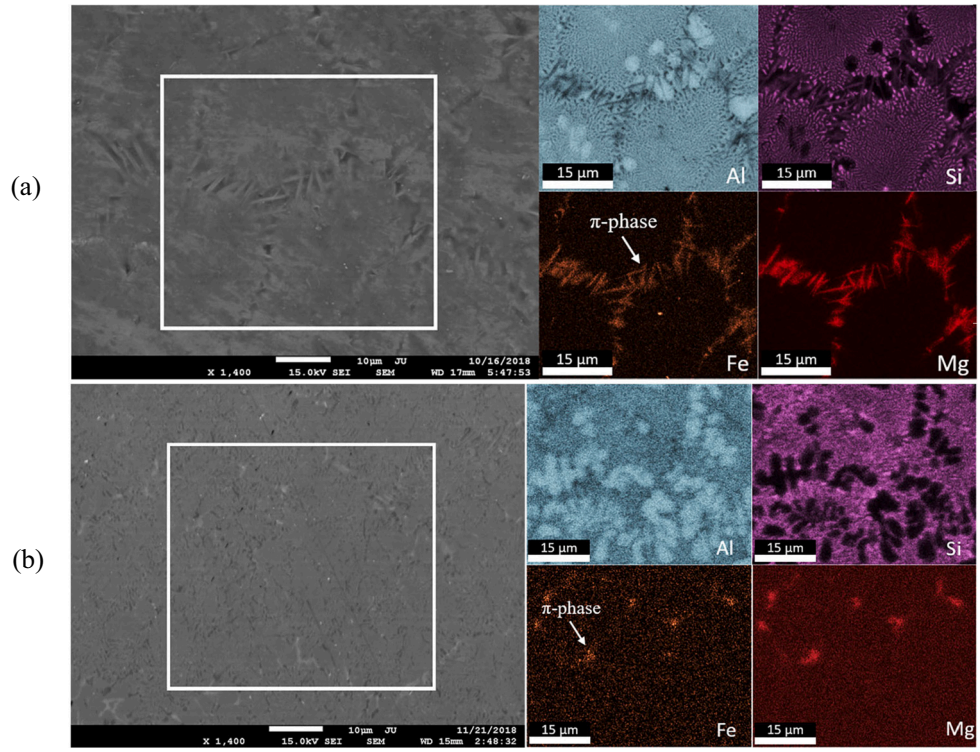

Fig. 1. SEM micrographs and EDXS elemental mapping of (a) unground surface, (b) mechanically ground surface.

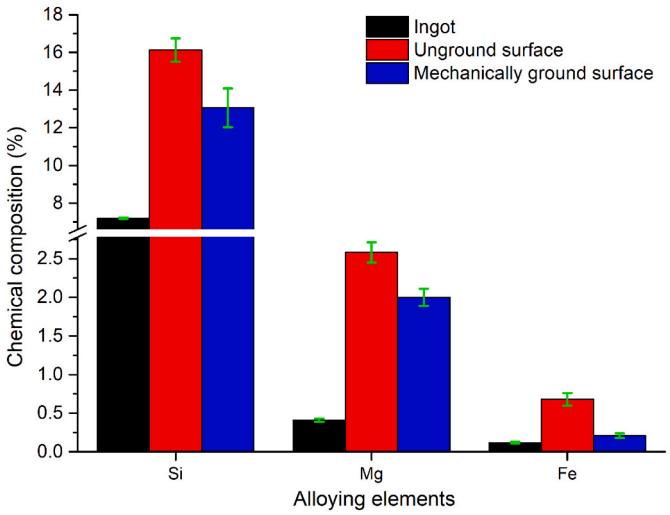

Fig. 2. Chemical composition (Si, Mg and Fe) of the ingot, unground surface and mechanically ground surface.

middle of the oxide layer in cross-section. The applied load for hardness testing was set at 5 mN, so that the diagonal of the indentation was one-third of the local oxide layer thickness or below.

2.5. Corrosion testing

The corrosion resistance of anodised samples was evaluated by electrochemical impedance spectroscopy (EIS) using an Ivium Vertex potentiostat. The anodised specimens were immersed in 3 wt-% NaCl solution at room temperature. The EIS spectra were recorded every 1 h within 12 h immersion, at an open-circuit potential with an amplitude of 15 mV and a frequency range from 10^{-1} Hz to 10^{5} Hz. In the current study, a minimum of three specimens of the same condition were tested to ensure the repeatability. All the EIS spectra were analysed and fitted by the ZSimp Win software program.

3. Results and discussion

3.1. Microstructure of Al—Si substrates

Fig. 1 compares the unground and mechanically ground surfaces of parts taken from near to the gate by SEM with EDXS mapping. It is noticeable that both unground and mechanically ground surfaces contain a high fraction of eutectic regions. However, the unground surface (Fig. 1a) shows enrichment of Fe-rich intermetallics, mainly π-AlFeMgSi phases, compared with the mechanically ground surface (Fig. 1b). The chemical composition of unground and mechanically ground surfaces taken from the same position was conducted by EDXS (Fig. 2) in the top view. The results indicate much higher alloying elements content, especially Si and Fe, on the unground surface than the mechanically ground surface. In rheocasting, due to the separation of the liquid phase from the solid phase during filling, the liquid phase containing higher alloying elements flows to the surface of the casting, resulting in the transverse macrosegregation by the presence of SLS layer [24,25]. Moreover, since the liquid phase has direct contact with the die, the interaction between the melt and die material (tool steel) results in the formation of Fe-rich intermetallics on the casting surface [26,27]. In the present study, the higher Fe content and therefore more Fe-rich intermetallics on the unground surface could be associated with the combination of transverse macrosegregation and the interaction between the melt and the die material.

3.2. Oxide layer characterisation

Fig. 3 depicts the in-beam backscattered SEM micrographs of the oxide layer in cross-section on selected unground and mechanically ground surfaces. As shown in Fig. 3, Si particles oxidised only minimally and remained embedded in the oxide layer [3], while the Fe-rich intermetallics could be partly/locally dissolved during anodising, leaving voids as the defects in the oxide layer [5,6,8].

To investigate the behaviour of Fe-rich intermetallic during anodising, the morphology (Fig. 4) and chemical composition (Table III) of Fe-rich intermetallics before and after anodising at 20 V for 300 s were studied and compared. As shown in Fig. 4b–d, instead of Fe-rich intermetallics (Fig. 4a), voids or defects were left on the surface after anodising for 300 s. Table III shows the EDXS analyses of different areas of different Fe-rich intermetallics before and after anodising for 300 s. The results demonstrated a clear decrease of Mg and Fe content, confirming a dissolution of Fe-rich intermetallics during anodising. Comparing the SEM micrographs of the oxide layer on unground and mechanically ground surfaces (Fig. 3), it was found that less voids derived from the Fe-rich intermetallic dissolution were observed in the oxide layer owing to lower Fe content in the surface after mechanical grinding.

3.3. Hardness

The hardness measurements of the anodised layer on unground and mechanically ground samples with different oxide layer thickness and anodising voltage are presented in Fig. 5. Hardness results indicated that the oxide layer on mechanically ground samples have a higher hardness than on unground samples when the oxide layer was produced at the

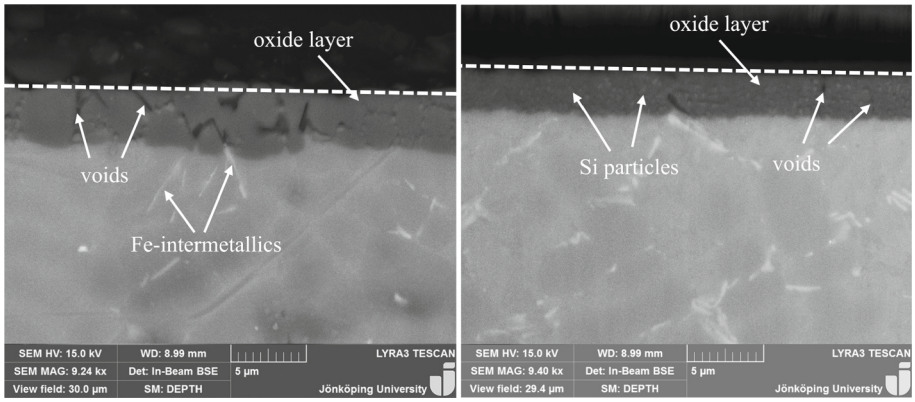

(a) (b)

Fig. 3. In-beam backscattered SEM micrographs of the oxide layer on (a) unground surface, (b) mechanically ground surface in cross-section.

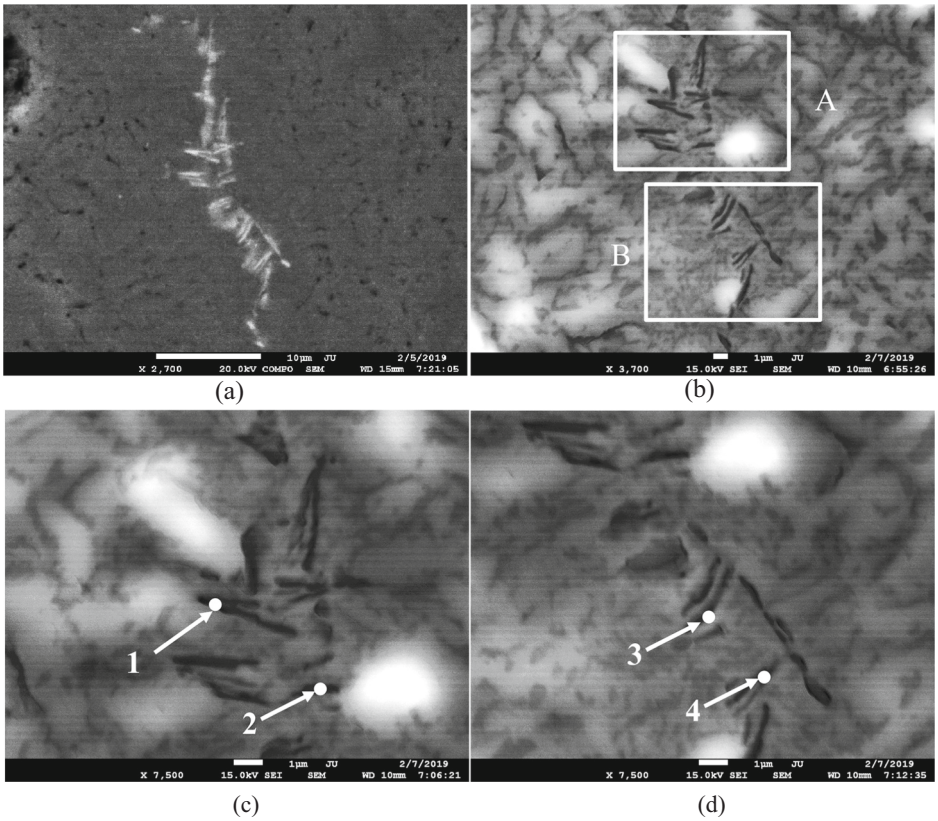

Fig. 4. SEM micrographs of Fe-rich intermetallics (a) before (b) after anodising at 20 V for 300 s; (c) and (d) correspond to framed area A and B after anodising.

Table III
EDXS analysis of different areas (in Fig. 4c & d) of different Fe-rich intermetallics before and after anodising at 20 V for 300 s.

No.	Anodising	Al (wt-%)	Si (wt-%)	Mg (wt-%)	Fe (wt-%)	O (wt-%)	S (wt-%)
1	Before	69.07	17.60	8.80	5.6	–	–
	After	51.15	15.50	2.67	1.96	26.01	2.04
2	Before	70.44	16.78	8.03	4.75	–	–
	After	53.42	14.52	1.63	0.41	27.60	2.42
3	Before	69.07	16.53	7.94	4.49	–	–
	After	53.42	11.36	2.33	0.65	29.92	2.3
4	Before	69.91	17.09	8.11	4.89	–	–
	After	51.08	11.46	2.55	0.88	31.7	2.33

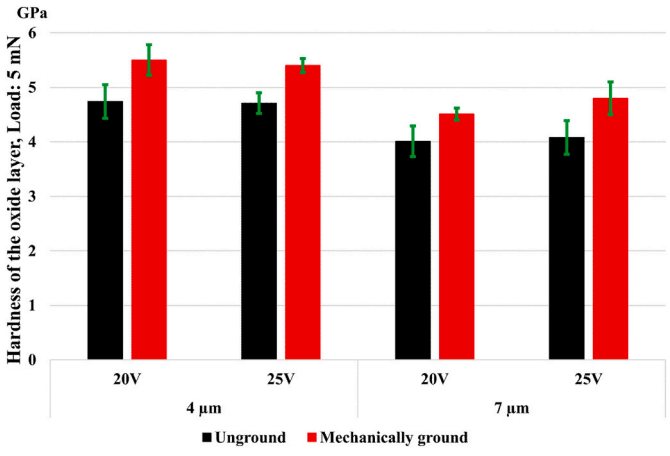

Fig. 5. Hardness of the oxide layer obtained at different voltages and thicknesses.

same thickness. As discussed previously, the mechanically grinding removes the casting skin which is enriched of Fe-rich intermetallics, and therefore less voids derived from the dissolution of Fe-rich intermetallics were obtained in the oxide layer. The increase of oxide hardness on mechanically ground samples could be attributed to the oxide layer with less voids as defects.

Comparing the hardness results of the oxide layers with two different thicknesses, it was found that the 4 µm-thick oxide layers have a higher hardness than the 7 µm-thick oxide layers. However, when the oxide layer has a similar thickness value, a similar hardness of the anodised layer was obtained despite the anodising voltages. Similar results were also presented in the previous study by Zhu et al. [28]. With the same surface condition, a thicker oxide layer was associated with an increase in the charge. The more charge passes through the surface; the more local heating is produced on the surface, leading to a coarser nano-porosity of the anodised layer leading to lower hardness [10]. Moreover, the decrease of the hardness at higher oxide thickness could also be associated with the defects in the oxide layer. The thicker the oxide layer is obtained, more oxide layer defects would be generated owing to the

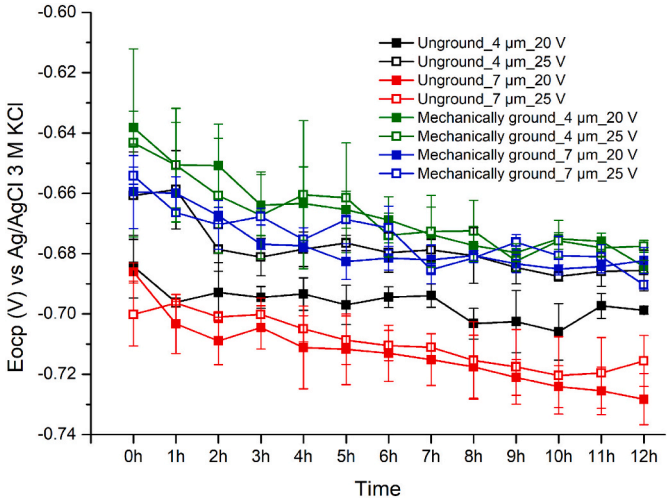

Fig. 6. OCP values of measured anodised samples with a function of immersion time.

release of intrinsic stress after anodising and the dissolution of Fe-rich intermetallics, leading to the decrease of oxide layer hardness [3].

3.4. Electrochemical characterisation

The corrosion resistance of anodised samples was evaluated by EIS in 3 wt-% NaCl solution during 12 h of immersion. The open-circuit potential (OCP) values for all measured samples as a function of immersion time are presented in Fig. 6. As shown in Fig. 6, all samples demonstrate a slight decrease of OCP values over time, and the unground samples depict relatively lower OCP values than the mechanically ground ones. Fig. 7 presents the Bode plot of EIS spectra after 1 and 12 h of immersion in the NaCl solution. The EIS spectra demonstrate a progressive corrosion attack, as the total impedance modulus decreases, as well as the phase angle depresses over time.

The comparison of impedance spectra of unground samples and mechanically ground samples after anodising shows that, with the similar anodised layer thickness, the mechanically ground samples demonstrate higher impedance modulus at the low-frequency range than unground samples. Moreover, comparing the two different thickness, it was found that the anodised samples with a thinner oxide layer (4 μm) show a higher impedance modulus at low frequencies than samples with a thick oxide layer (7 μm) both for unground and mechanically ground samples.

Impedance spectra were fitted by the equivalent circuit, $R_{el}(CPE_{ox}$-$R_{ox})(CPE_{dl}R_{po})$, in order to obtain the quantitative information for corrosion protection performance of the oxide layer. The same circuit was also used in previous studies [2,7]. In the circuit, R_{el} represents the resistance of the electrolyte, R_{ox} and R_{po} indicate the porous oxide layer resistance and the polarisation resistance, correspondingly [2,7]. In the present study, the capacitive behaviour of the oxide layer and the electrical double layer were represented and simulated by two constant phase elements (CPE), CPE_{ox} and CPE_{dl}, respectively [2,7]. A good fitting of measured (points) and fitted (grey lines) spectra was evident in Fig. 7. The average values of polarisation resistance (R_{po}) and "pre-factor" Q_{dl} were summarised and presented in Fig. 8 with error bars refer to the standard deviation, and Table IV demonstrates the interval values of n for CPE_{dl}.

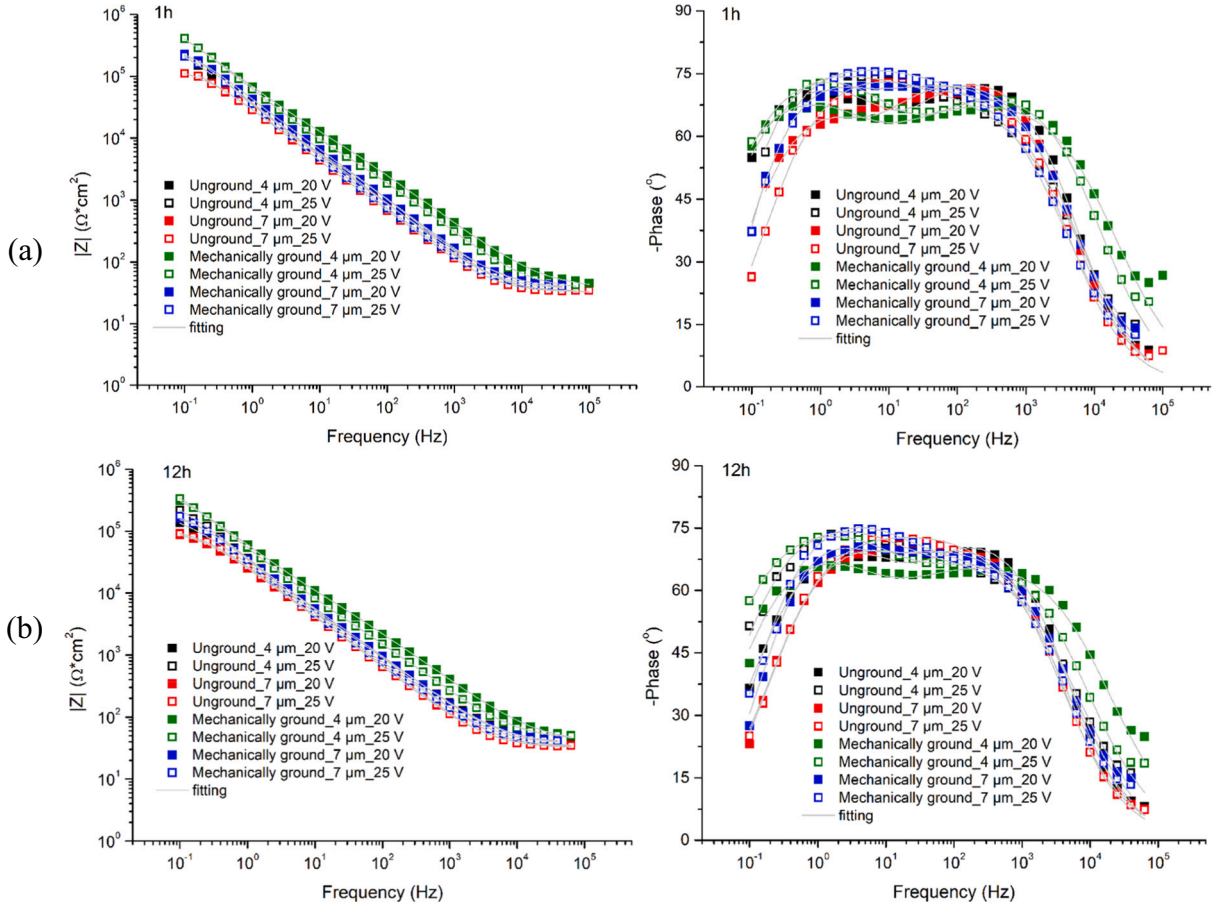

Fig. 7. Bode plot of impedance spectra of selected anodised samples after (1) 1 h and (b) 12 h of immersion.

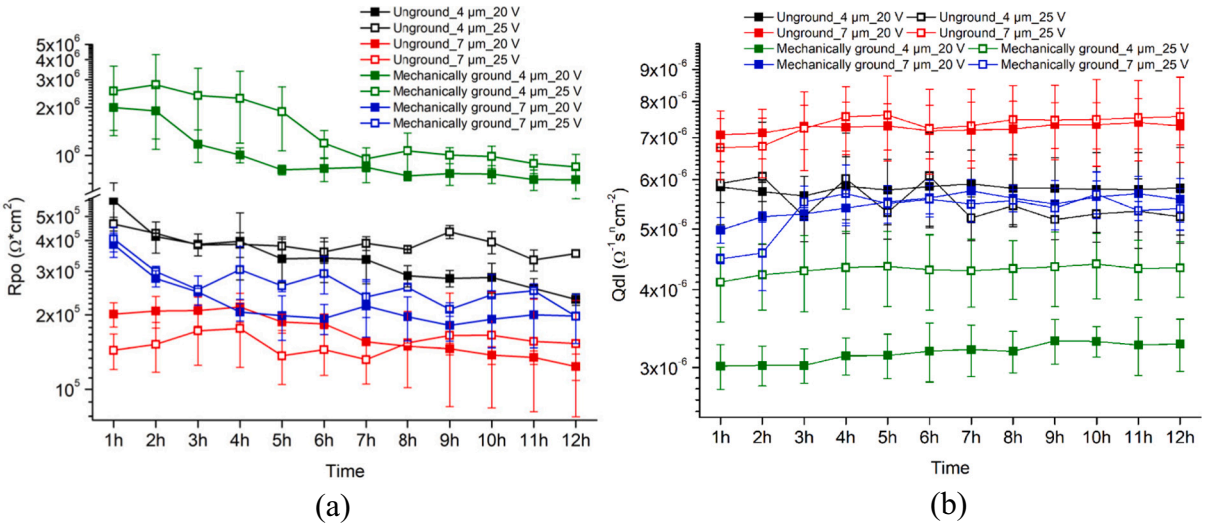

Fig. 8. Results of equivalent circuits fitting (a) R_{po}, (b) Q_{dl}.

Table IV
Values of n for CPE_{dl}.

Measured anodised samples	Value of n for CPE_{dl} with 12 h
Unground _4 µm_20 V	0.83–0.94
Unground _4 µm_25 V	0.83–1.00
Unground _7 µm_20 V	0.83–0.86
Unground _7 µm_25 V	0.79–1.00
Mechanically ground_4 µm_20 V	0.71–0.95
Mechanically ground _4 µm_25 V	0.83–0.87
Mechanically ground _7 µm_20 V	0.85–0.95
Mechanically ground _7 µm_25 V	0.88–1

As shown in Fig. 8, that mechanically ground samples have higher R_{po} values and lower Q_{dl} values than unground samples, especially when the oxide layer thickness is 4 µm. The presence of Fe-rich intermetallics on the surface reduces the corrosion resistance of the oxide layer, as they were partly dissolved, leaving voids in the oxide layer [5,6,8]. In the current study, the mechanically grinding contributes to reducing the Fe content and Fe-rich intermetallics on the surface, and therefore less voids due to the dissolution of Fe-rich intermetallics were obtained in the oxide layer, which could result in better corrosion protection of the oxide layer.

The fitting results also show that the oxide layer thickness plays an important role in the corrosion protection of the anodised layer. Comparing the R_{po} and Q_{dl} values of the anodised samples with different oxide thickness, the samples with a thinner oxide layer is associated with higher R_{po} values and lower Q_{dl} values than samples with a thicker oxide layer. Similar results were also presented in a previous work by Zhu et al. [28] where it was reported that a thicker oxide layer contains more defects or cracks, which could be a result of the release of stress at the Si oxide interfaces after anodising. Moreover, as the Fe-rich intermetallics could be partly dissolved during anodising, a thinner oxide layer could limit the possibility of the oxide front reacting with the Fe-rich intermetallic, resulting in less cracks in the oxide layer.

3.5. Corrosion attack characterisation

Selected representative anodised samples were continuously immersed in 3 wt-% NaCl solution for 72 h for corrosion attack characterisation. Fig. 9 shows the corrosion pits on the unground and mechanically ground samples, and it appears that the corrosion attack penetrated the oxide layer and was localised on the eutectic region with the presence of Fe-rich intermetallic in Al—Si matrix. FIB polishing was performed to slice the corrosion pit in a cross-section view to investigate the corrosion propagation path, as shown in Fig. 10. The SEM micrographs with EDXS maps show intensive corrosion of the Al—Si matrix enclosed by Fe-rich intermetallics under the anodised layer.

An oxide layer was generated on Al—Si substrates with the presence of oxide layer defects resulting from the dissolution of Fe-rich intermetallic during anodising (Fig. 11a–b). With the immersion of anodised samples in NaCl solution, the NaCl solution could penetrate to Al—Si matrix through oxide layer defects (Fig. 11c). In the current study, unground, as-cast surfaces provide more channels for the penetration of NaCl solution due to the Fe-rich defects compared to ground surfaces. With the presence of nobler Fe-rich intermetallics beneath the oxide layer, a galvanic couple forms with the less noble Al—Si matrix, resulting in galvanic corrosion beneath the anodised surface [6,19,29,30] (Fig. 11c–d). By the dissolution of the substrate, the above oxide layer collapsed, as shown as corrosion pits on the surface (Fig. 11d).

4. Conclusions

During rheocasting of Al—Si alloys, the component's surface can be enriched in Fe-rich intermetallics due to the combination of the surface liquid segregation and the interaction with die material. The enrichment of Fe-rich intermetallics has a strong influence on the quality of the anodised layer and its durability.

The Fe-rich intermetallics partially dissolve during the anodizing, leaving voids in the oxide and facilitating the propagation of corrosion attack into the Al—Si matrix and the corrosion of the Al—Si matrix when they were displayed under the interface of the oxide layer and Al—Si matrix. The removal of casting skin by mechanically grinding decreases the Fe content and Fe-rich intermetallics on the casting surface, resulting in improved oxide layer quality.

Moreover, in this study, it was found that the oxide layer thickness also has a big impact on the hardness of the anodised layer. A decrease of oxide layer thickness improves the hardness and corrosion protection of the oxide layer, and a combination of the thin oxide layer and the removal of casting skin makes the oxide layer harder and more resistant to corrosion.

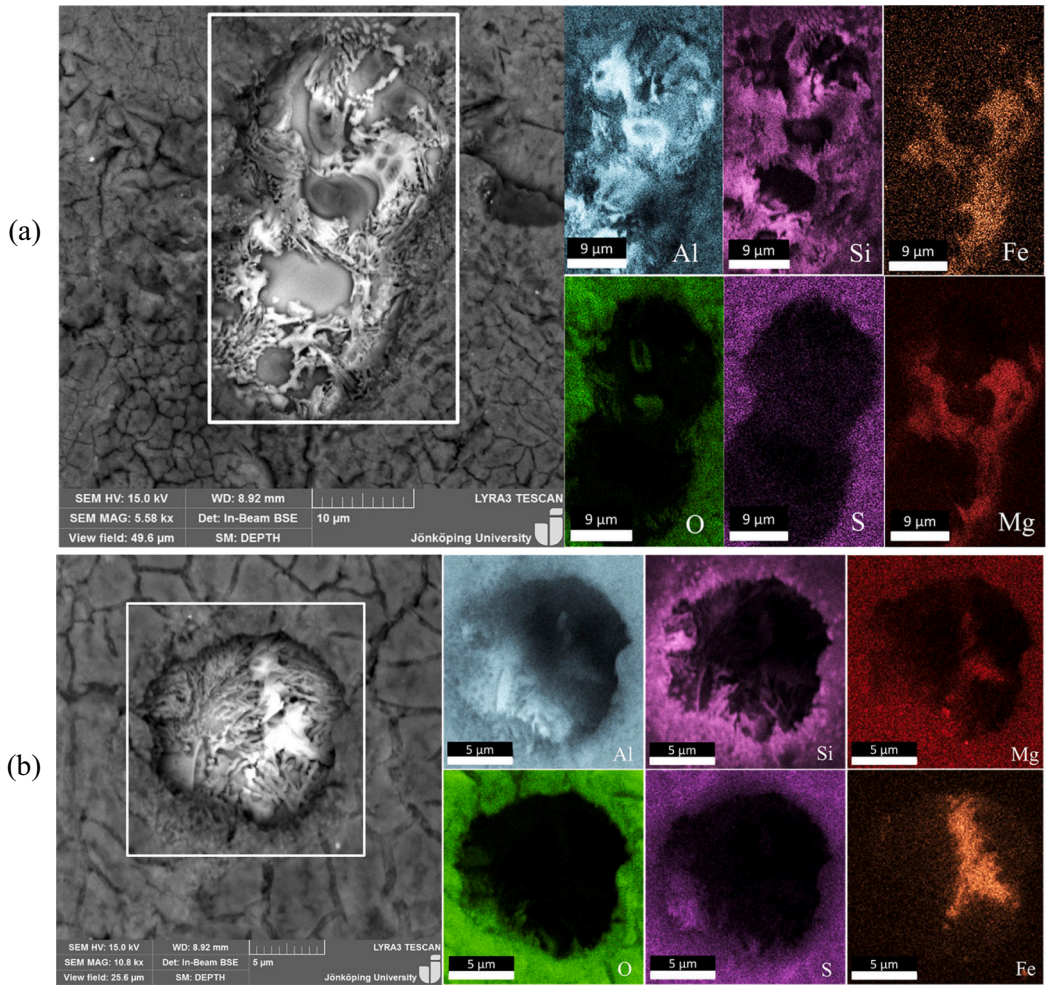

Fig. 9. SEM micrographs and EDXS element mapping of corrosion pits on (a) unground surface and (b) mechanically ground surface in top view.

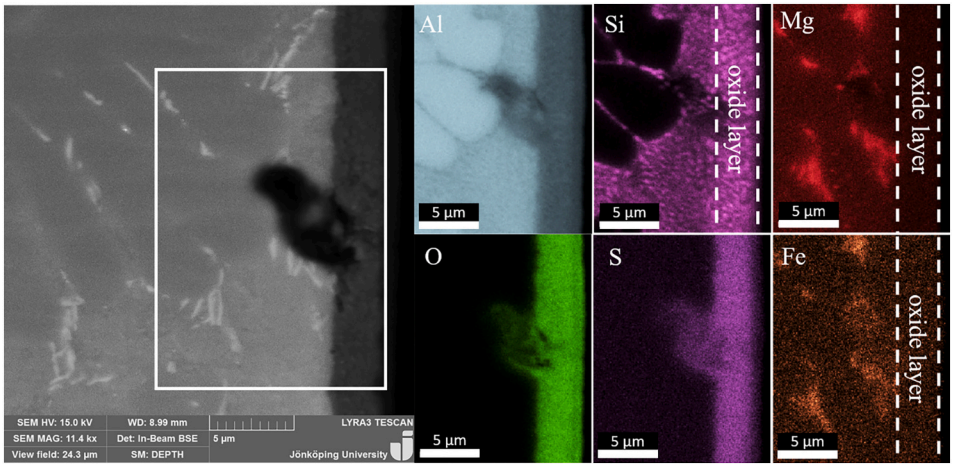

Fig. 10. SEM micrographs and EDXS element mapping of corrosion pit in cross-section.

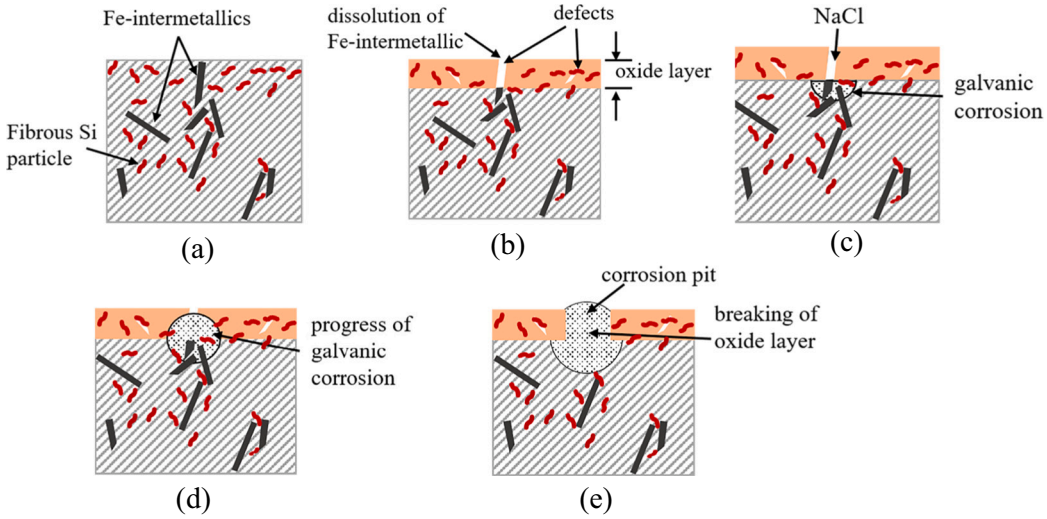

Fig. 11. The proposed formation of corrosion pit in anodised Al—Si sample: (a) before anodising, (b) after anodising, (c) formation of galvanic corrosion, (d) progress of the galvanic corrosion, (e) formation of corrosion pits.

CRediT authorship contribution statement

Baiwei Zhu and Caterina Zanella conceived and designed the experiments;
Baiwei Zhu performed the experiments;
Baiwei Zhu and Caterina Zanella analysed the data;
Baiwei Zhu and Caterina Zanella wrote the paper.

Declaration of competing interest

The authors have no conflict of interest to disclose.

The work was funded by the Swedish Knowledge Foundation, KKstiftelsen, with grant number No. 20170066, which is gratefully acknowledged.

Acknowledgement

The present work was financially supported by the KK-foundation (CompCast Plus Project No. 20170066), who is gratefully acknowledged. The authors would like to thank Jorge Santos for his assistance with casting experiments and Dr. Fengxiang Lin for her assistance with SEM preparation and analyses.

References

[1] L.E. Fratila-Apachitei, H. Terryn, P. Skeldon, G.E. Thompson, J. Duszczyk, L. Katgerman, Electrochim. Acta 49 (2004) 1127–1140.
[2] B. Zhu, M. Fedel, N.-E. Andersson, P. Leisner, F. Deflorian, C. Zanella, J. Electrochem. Soc. 164 (2017) C435–C441.
[3] B. Zhu, S. Seifeddine, P.O.Å. Persson, A.E.W. Jarfors, P. Leisner, C. Zanella, Mater. Des. 101 (2016) 254–262.
[4] M. Aggerbeck, S. Canulescu, K. Dirscherl, V.E. Johansen, S. Engberg, J. Schou, R. Ambat, Surf. Coat. Technol. 254 (2014) 28–41.
[5] H. Wu, Y. Ma, W. Huang, X. Zhou, K. Li, Y. Liao, Z. Wang, Z. Liang, L. Liu, J. Electrochem. Soc. 165 (2018) C573–C581.
[6] F. Zhang, J.-O. Nilsson, J. Pan, J. Electrochem. Soc. 163 (2016) C609–C618.
[7] B. Zhu, M. Fedel, N.-E. Andersson, P. Leisner, F. Deflorian, C. Zanella, Joint European Corrosion Congress 2017, EUROCORR 2017 and 20th International Corrosion Congress and Process Safety Congress 2017, Asociace Koroznich Inzenyru z.S.- AKI - Czech Association of Corrosion Engineers, Prague, Czech Republic, 2017, pp. 27–39.
[8] B. Zhu, S. Seifeddine, A.E.W. Jarfors, P. Leisner, C. Zanella, 15th International Conference on Semi-Solid Processing of Alloys and Composites, Shenzhen, China, 2018.
[9] K. Chauke, H. Möller, U.A. Curle, G. Govender, Mater. Sci. Forum 765 (2013) 658–662.
[10] T. Aerts, T. Dimogerontalis, I. De Graeve, J. Fransaer, H. Terryn, Surf. Coat. Technol. 201 (2007) 7310–7317.
[11] L.E. Fratila-Apachitei, I. Apachitei, J. Duszczyk, J. Appl. Electrochem. 36 (2006) 481–486.
[12] D. Kuhn, A. Martin, C. Eckart, M. Sieber, R. Morgenstern, M. Hackert-Oschätzchen, T. Lampke, A. Schubert, 2017 IOP Conf. Ser.: Mater. Sci. Eng, IOP Publishing Ltd, Chemnitz, Germany, 2017.
[13] R. Morgenstern, D. Nickel, D. Dietrich, I. Scharf, T. Lampke, Mater. Sci. Forum 825-826 (2015) 636–644.
[14] T. Tamamoto, H. Tanaka, M. Fujita, H. Asoh, S. Ono, J. Jpn. Inst. Light Metals 60 (2010) 602–607.
[15] M. García-Rubio, M.P. de Lara, P. Ocón, S. Diekhoff, M. Beneke, A. Lavía, I. García, Electrochim. Acta 54 (2009) 4789–4800.
[16] M. Jariyaboon, P. Møller, R.E. Dunin-Borkowski, R. Ambat, Anti-Corros. Methods Mater. 58 (2011) 173–178.
[17] M. Mohedano, E. Matykina, R. Arrabal, B. Mingo, A. Pardo, Appl. Surf. Sci. 346 (2015) 57–67.
[18] L. Ceschini, I. Boromei, A. Morri, S. Seifeddine, I.L. Svensson, Mater. Des. 36 (2012) 522–528.
[19] M. Eslami, M. Payandeh, F. Deflorian, A.E.W. Jarfors, C. Zanella, Metals 8 (2018) 209–226.
[20] B. Mingo, R. Arrabal, A. Pardo, E. Matykina, P. Skeldon, Mater. Charact. 112 (2016) 122–128.
[21] S. Wernick, R. Pinner, P.G. Sheasby, The Surface Treatment and Finishing of Aluminum and its Alloys, 5 ed., Finishing Publications LTD, Teddington, Middlesex, England, 1987.
[22] M. Wessén, H. Cao, J. Metallur. Appl. Surf. Sci. 25 (2007) 22–28.
[23] E. Sjölander, S. Seifeddine, Mater. Sci. Eng. A 528 (2011) 7402–7409.
[24] H. Kaufmann, W. Franger, U. Galovsky, P.J. Uggowitzer, in: H. Kaufmann (Ed.), 2nd International Light Metals Technology Conference, LKR-Verlag, St, Wolfgang, Austria, 2005, pp. 169–177.
[25] H.I. Laukli, C.M. Gourlay, A.K. Dahle, Metall. Mater. Trans. A 36 (2005) 805–818.
[26] Q. Han, S. Viswanathan, Metall. Mater. Trans. A 34 (2003) 139–146.
[27] S. Shankar, D. Apelian, Metall. Mater. Trans. B Process Metall. Mater. Process. Sci. 33 (2002) 465–476.
[28] B. Zhu, C. Zanella, Mater. Des. 173 (2019).
[29] R. Arrabal, B. Mingo, A. Pardo, M. Mohedano, E. Matykina, I. Rodriguez, Corros. Sci. 73 (2013) 342–356.
[30] D.M. Sun, Y.M. Jiang, Q.W. Xiang, C. Zhong, J. Gong, H. Zhang, J. Li, Mater. Corros. 61 (2010) 105–110.